Proc. Natl. Acad. Sci. USA
Vol. 94, pp. 7927–7931, July 1997
Biophysics

Detection of single-molecule interactions using correlated thermal diffusion

A. D. MEHTA, J. T. FINER, AND J. A. SPUDICH†

Departments of Biochemistry and Developmental Biology, Beckman Center, Stanford University School of Medicine, Stanford, CA 94305

Contributed by James A. Spudich, May 16, 1997

ABSTRACT **Observation of discrete, single-molecule binding events allows one to bypass assumptions required to infer single-molecule properties from studies of ensembles of molecules. Optically trapped beads and glass microneedles have been applied to detect single-molecule binding events, but it remains difficult to identify signs of binding events given the large displacements induced by thermal forces. Here, we exploit thermal diffusion by using correlation between motion of optically trapped beads attached to both ends of a single actin filament to track binding events of individual myosin molecules. We use correlated diffusion to measure the stiffness of a single myosin molecule and estimate its thermal fluctuation in a poststroke state as comparable in amplitude to the measured stroke distance. The use of correlated diffusion to measure kinetics of single-molecule interactions and the stiffness of the interacting moieties should be applicable to any pair of interacting molecules, and not limited to biological motors.**

The ultimate goal in molecular biophysics is the direct observation of a single molecule moving through intermediates in a chemical cycle. A significant step to this end involves real-time detection of individual binding events. Important questions include single-molecule kinetics of state transitions as well as the physical compliance of the proteins involved and the connections between them.

Atomic force microscope cantilever tips have been used to place strain on individual antibody–antigen contacts and examine their dissociation times (1, 2). However, experiments with these relatively stiff probes involve significant mechanical perturbation of the protein linkage. Weak probes such as optical tweezers (3–6) and glass microneedles (7, 8) have been used to observe discrete probe deflections produced by individual molecular motors, but examination of probe position may not be as useful to study interactions not producing directed movement.

In the general case, one seeks to detect binding, characterize the connection, and detect dissociation without perturbing the interaction. This task is further complicated by the large amount of thermal diffusion, often many times the size of the involved proteins, experienced by probes sufficiently compliant to avoid perturbing a single molecule connection. In the study of myosin binding to actin, suppression of this diffusion has been used to identify binding events, including those producing no net displacement of the probe (5). If the protein of interest and the mechanical probes are by far the most compliant elements in the system, this method seems the most reliable demonstrated to date. However, compliance elsewhere in the system can make this fall in diffusion amplitude modest, rendering some binding events indistinguishable from baseline fluctuations (9).

We describe here a new and general method for examining single molecular interactions. The method involves simultaneous observation of thermal diffusion of optically trapped beads attached to both ends of a single filamentous polymer (Fig. 1). We illustrate the method using the interaction of myosin with actin. Experiments with actin have involved attached probes either to one or both ends of a single filament in efforts to examine mechanical stiffness in a strained linkage to myosin (11) or movements and tension transients created by myosin binding (4–9). However, these experiments have not included simultaneous imaging and high-resolution position detection at both the barbed and the pointed ends of the polar actin filament.

In the highly overdamped regime of low Reynold's number physics, a trapped bead experiences thermal forces, resistance from the optical trap, and viscous drag from movement through an aqueous medium. When two probes are connected by a filament stretched taut, heated water molecules colliding with one probe will affect movement of the other probe through the connecting polymer and any compliant linkage separating them. Hence, a strong statistical correlation appears between thermal diffusion at the two ends of the filament (Fig. 1 *a–c*). Once a relatively noncompliant molecule, which is attached to a nearby surface, binds somewhere along the polymer and clamps its position, it immediately breaks the coupling between diffusion at filament ends (Fig. 1 *d–f*). Hence, by tracking statistical correlation between movement of the ends, one can detect binding events that may not be visible unambiguously in the probe position data.

MATERIALS AND METHODS

The apparatus was configured as previously described (4, 12), using two independent optical traps to constrain the motion of micrometer-sized beads attached to either end of an actin filament. The filament is then moved into close proximity of silica beads fixed to a microscope coverslip and sparsely decorated with a myosin fragment, known to bind and cause directed movement of actin. All experiments reported here were performed with heavy meromyosin. Unlike previous experiments (4, 5, 7–9), the brightfield image light was split into two paths, and the beads at both ends of the actin filament were imaged simultaneously with nanometer and millisecond resolution using quadrant photodetectors. The quadrant detectors used to measure bead position (12) have 15-kHz bandwidth, high enough to track the optically trapped beads over nearly the full frequency range of their motion. Splitting of the image light into two detectors reduced intensity and thus increased the relative contribution of shot noise to the position signal. To recover high signal to noise levels, we used a multimode diode laser operating at wavelength 830 nm to illuminate the specimen slide. The illumination source was selected based on its intensity level and stability, linearity of the position-detection signal, and a lack of statistical correlation between perceived bead motion along perpendicular axes in the specimen plane. To eliminate speckle, the beam was passed through a multimode optical fiber with a mode scrambler and the laser was operated just below the lasing threshold current. The traces occasionally showed very slow drifting, as observed previously in laser-based brightfield imaging (8). Events so effected

The publication costs of this article were defrayed in part by page charge payment. This article must therefore be hereby marked "*advertisement*" in accordance with 18 U.S.C. §1734 solely to indicate this fact.

†To whom reprint requests should be addressed.

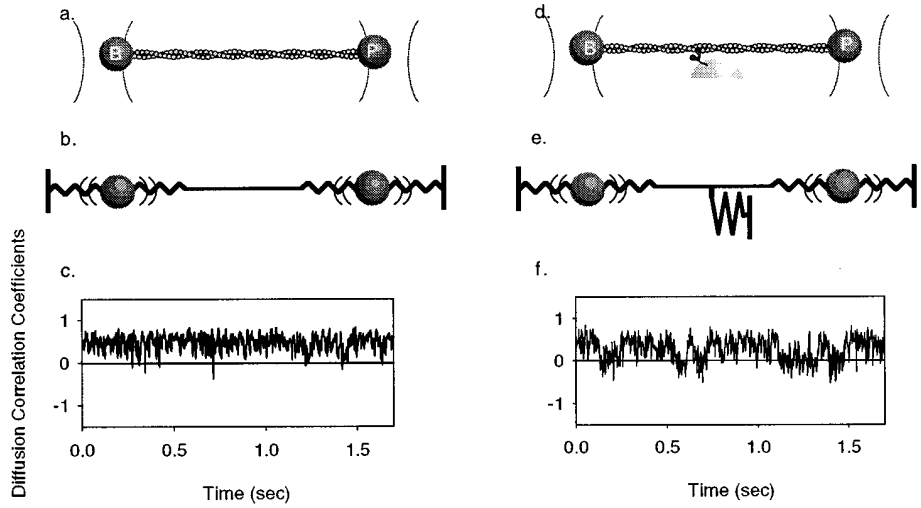

FIG. 1. (*a*) An actin filament held taut by optical trapping of beads attached to both ends. (*b*) Schematic representation of the elastic constraints in the system, with Hookean traps and assumed Hookean-compliant connections between the optically trapped beads and the filament. The compliance of the filament itself (10) is about 1,000 times less than that of the bead-to-bead linkage we observe, indicating the presence in series of weaker elements, probably the bead–filament linkages. The motion of each bead depends on trap strength, viscous drag, and the motion of the other bead "felt" through a compliant attachment. (*c*) Diffusion correlation coefficients between diffusive motion of the two beads along the filament axis measured every 5 ms for a 1.7-s interval. Despite statistical fluctuation, the values remain centered around 0.4 to 0.5. (*d*) A surface-attached myosin binds to the filament, schematically illustrated in *e*. Because the actin filament center is now linked to the myosin-bound surface through a relatively stiff contact, motion at one filament end propagates only weakly to the other. Consistent with this prediction, we show in *f* observed transient drops in correlation between diffusion of the two beads. We interpret these drops to reflect myosin binding to the actin filament.

should be eliminated using our scoring criteria (see *Appendix*). The signals have been digitally sampled at 10 kHz. Both traps have stiffness of around 0.03 pN/nm, as measured using both rms noise amplitude and by fitting the 3-dB corner frequency to Lorentzian power spectra of diffusive motion when the bead is trapped 5 μm away from the slide surface, as shown previously (3).

RESULTS AND DISCUSSION

When the actin filament was stretched to a tension of around 3 pN, significant statistical correlation appeared between diffusion of the two beads moving along the filament axis (Fig. 1 *a–c*). When the surface was sparsely decorated with the myosin fragment heavy meromyosin, we observed a number of events in which the diffusion correlation coefficient dropped to near zero (Fig. 1 *d–f*), rising back to its previous value after 88 ms on average. We assume these transient drops in diffusion correlation reflect myosin-binding events. We expect the average duration measurement to be an overestimate because fast transients will escape detection. Assuming a single exponential distribution created by a single step detachment, the statistically reliable subset of the data (duration range, 30–300 ms)‡ indicates the actual mean time is around 65 ms with an uncertainty range of 55–80 ms. The data could not be fit (to a reduced χ^2 of 1) as a sequential process of two comparable steps, arguing that the transients we observe involve only one myosin head. The predicted mean duration of single-molecule myosin interactions is approximately 50 ms, given experimental conditions of 5 μM ATP and the second order rate constant for ATP binding to actomyosin (13).

Many of these transient diffusion correlation losses accompanied clear deflection of bead position (Fig. 2 *a* and *c*) or temporary decreases in the amplitude of Brownian motion (Fig. 2 *b* and *d*), also expected because the myosin attachment increases the constraints on bead diffusion (4, 5). Event durations showed no correlation with amplitude or direction of bead position shift,

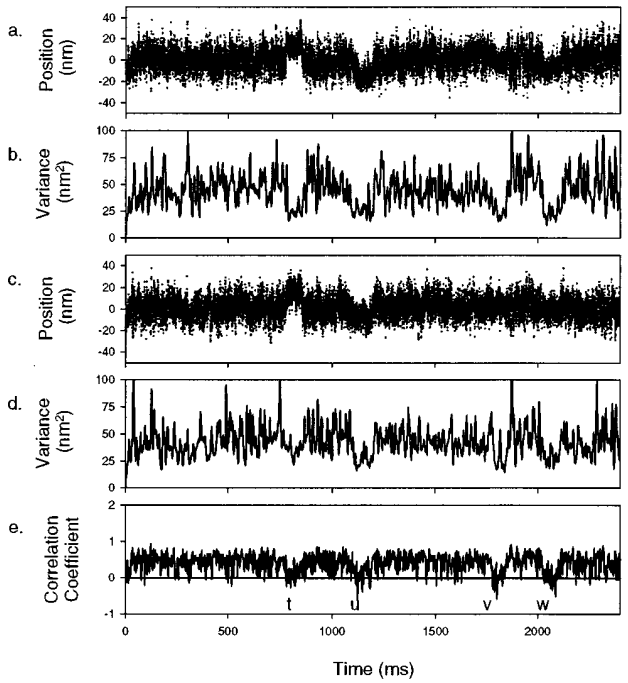

FIG. 2. Sample data traces. *a* and *c* show raw position data for beads at the actin filament pointed and barbed ends (beads P and B), respectively. *b* and *d* provide computation of bead P and B position variance for every 15-point (1.5-ms) interval. To clarify regions of suppressed position variance, these traces have been processed, using single-pole Butterworth filters of 100 Hz bandwidth. *e* provides a running measure of linear correlation between motions of the two beads. Each point represents correlation between 35 points (3.5 ms) of position data. Drops in diffusion correlation correspond with drops in position variance on both beads, although the latter are sometimes difficult to see. In most binding events, deflections are not clearly observed in the raw data trace, as observed previously (5). In general, the drop in diffusion correlation provided the least ambiguous signal of a myosin-binding event. In tabulating these data, we first examined nothing but diffusion correlation traces such as *e*, marking here the four drops in correlation labeled t, u, v, and w. All traces combined generated 387 such events, averaging 88 ms in duration.

‡Only 10 events exceed 300 ms in duration, so the distribution over 300 ms is not statistically significant. We do not believe all the events under 30 ms could be scored. Kinetic parameter fits remain consistent if we use 40 ms as the low end limit.

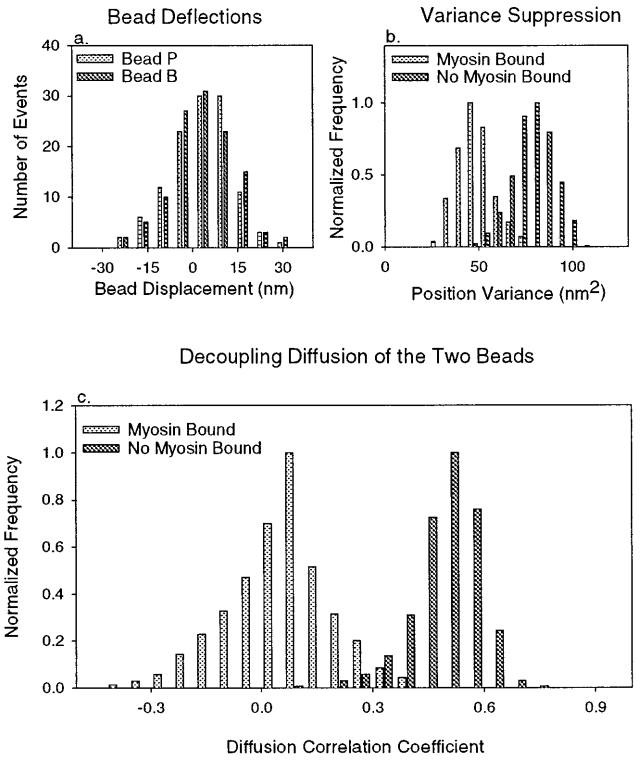

FIG. 3. (*a*) Tabulation of bead deflections, after elimination of outliers in the variance distributions (see *Appendix*) and including only binding events bordered by 100-ms baseline regions with mean positions less than 3 nm apart. The remaining 112 points have been corrected for displacement absorbed by compliant bead/filament connections. Independent measurements of the stroking distance on either side of the filament yield distributions centered about 4.1 ± 0.8 nm for bead B and 5.3 ± 0.9 nm for bead P. The uncertainties are calculated by the method of maximum likelihood, assuming that all errors are statistical, and do not account for possible systematic errors such as that which might be caused by the random relative orientation of surface-bound myosin and the actin filament. Both distributions have a variance of 79 nm^2, the same as the variance of baseline Brownian motion, consistent with the postulate that variance in bead deflection amplitudes is caused by myosin binding to the actin filament anywhere in its range of diffusive motion with equal probability (5). Total position variance within each event and 100-ms baseline interval was measured. *b* shows position variance distributions for bead P, after removal of outliers (see *Appendix*). Myosin clearly suppresses the position variance, and the values with myosin bound are centered about 48.3 ± 0.5 nm^2 and 46.3 ± 0.5 nm^2 for beads P and B (not shown), respectively. All uncertainties are computed using a maximum likelihood fit to a normal distribution and computing the change in mean, causing an increase of reduced χ^2 by 1. Using equipartition of energy (3), we computed the elastic constraints upon beads P and B as 0.08 pN/nm and 0.09 pN/nm. Subtracting trap strength, we estimated the elements connecting each optically trapped bead to the slide surface through the myosin molecule to have combined stiffness of around 0.05 and 0.06 pN/nm for the actin/bead assembly used in this experiment. The 0.027-pN/nm series combination of these agrees with the value computed from correlated diffusion (Fig. 4 legend), indicating that the bead-to-filament connection is much weaker than all other elements in the optically trapped bead-to-surface linkage. *b* also shows the position variance distribution for bead P without attached myosin. Such distributions are centered about 79 nm^2 and 87 nm^2, respectively, again with very small uncertainties, indicating respective constraints of around 0.05 pN/nm on each bead. Position variances in regions just before myosin binding and just after release were uncorrelated, indicating that the distribution spread probably reflects statistical fluctuation rather than actual changes in the elasticity of the system. With no myosin attached to the actin, each bead is constrained by a parallel combination of its trap and the other trap in series with the link between the beads. The values one computes from these parameters are 0.05 and 0.04 pN/nm, which are very close to those measured. (*c*) The distribution of measured diffusion correlation coefficients, each for a 100-ms interval preceding or following each myosin-binding event, after outliers in the position variance distributions have been removed (Fig. 2 legend). Independent analysis of regions before and after the events gave two essentially identical diffusion correlation coefficient distributions. With no myosin bound, the mean value is 0.45 with an uncertainty of 0.005. The distribution of measured correlation diffusion coefficients in regions where a myosin is bound, after removal of outliers in the position variance distributions, is centered at about 0.05 with an uncertainty of 0.01. The uncertainty range assumes that errors in the data are statistical and not systematic.

amount of variance loss, or the value of the correlation coefficients between thermal diffusion of the two beads. Without the diffusion correlation data (Fig. 2*e*), the position and variance alone often did not provide sufficient confidence to distinguish a binding event from background noise. In general, the loss of correlated diffusion provided the least ambiguous signal that a myosin molecule had bound to the actin filament. Moreover, the bead movements remained correlated most of the time, indicating that the isolated transient drops likely involved only one molecule. We applied additional criteria to eliminate traces affected by low frequency drift before tabulating myosin-induced bead deflections (see *Appendix*).

Comparison of bead position variance while myosin is bound with that when myosin is not bound showed a downward shift in distribution (Fig. 3*b*). Note that the distribution reflecting bound myosin and that reflecting no bound myosin have significant overlap, emphasizing the importance of the drop in correlated diffusion for identifying binding events. These data provide the compliance of the optically trapped bead to surface connection, which is a series combination of the bead/actin link, the internal myosin stiffness of interest, and the myosin/surface attachment. For the given data (Fig. 3*b*), the linkages have stiffness of 0.05 pN/nm and 0.06 pN/nm at the barbed and pointed filament ends, respectively. These numbers are an order of magnitude below the range expected to characterize myosin and its linkage to actin, so the stiffness of the myosin molecule is likely obscured by a much weaker compliant element connecting the bead to the actin filament. The problem of weaker compliant elements in series affects any attempt to estimate myosin stiffness by direct measurement of a stress–strain curve.

The relative weakness of the bead/filament links allows a single myosin molecule to decouple diffusion of the two beads almost completely, creating a clear signal reflecting the binding event. We measured bead position in binding event areas relative to baseline and corrected them for displacement absorbed by the compliant bead–actin linkages. Independent estimates of the myosin working stroke from movement of beads at the barbed and pointed ends of the polar actin filament are 4.9 ± 0.5 nm and 6.5 ± 0.4 nm, respectively (errors correspond to increase of χ^2 by 1, method of maximum likelihood). If we tabulate only events bordered by baseline regions with mean positions less than 3 nm apart, we estimate the stroke to be 4.1 ± 0.8 nm and 5.3 ± 0.9 nm at the barbed and pointed ends, respectively (Fig. 3*a*). These values could be underestimates, given that the relative orientation of myosin and the actin filament axis is randomly distributed. Nonetheless, the broad-band, dual-bead detection system used here makes these values more precise than our prior measurements (4), which served primarily to distinguish between stroke distance values of around 10 nm (15–17) and much higher estimates (14, 18, 19), within acknowledged resolution limits (4). The current values are consistent with structure-based predictions (20) and with those reported by Molloy *et al.* (5), except that our distribution of myosin-induced bead deflections shows no hint of any second peak at a higher value. The distribution width of the measured bead deflections matches within 10% the distribution width of bead position at the baseline, consistent with the expected randomizing effect of thermal noise (5) and inconsistent with results using a method of mean variance analysis (9).

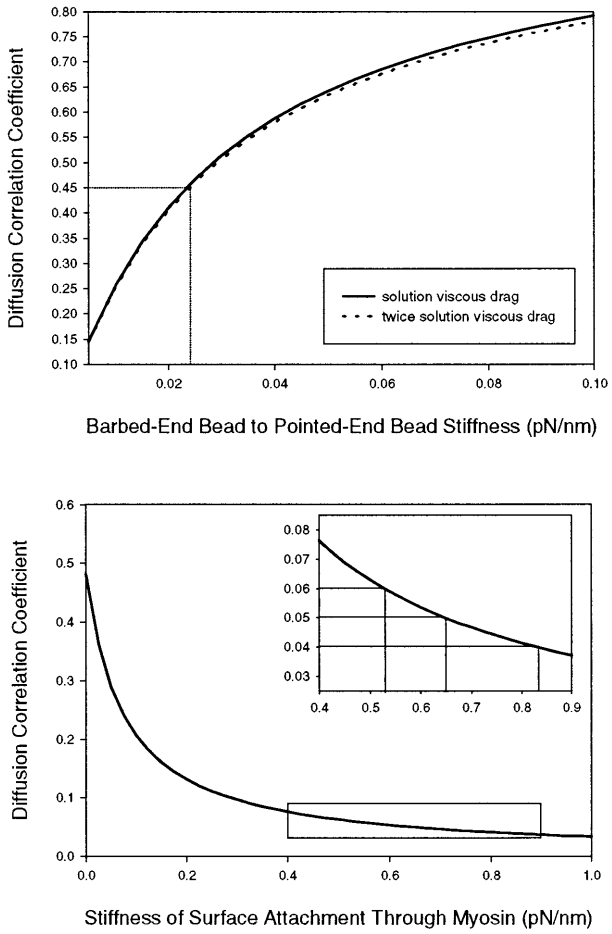

FIG. 4. In the heavily overdamped environment of an optically trapped bead, the equation of motion is $F_u(t) - \alpha u(t) - b\, du(t)/dt + [w(t) - u(t)]\gamma_u = 0$, where $F_u(t)$ refers to thermal forces upon the bead, α is trap stiffness, $u(t)$ refers to bead position relative to trap position, b is the coefficient of viscous drag, $w(t)$ is the position of the myosin-binding site on the actin filament relative to its equilibrium value, and γ_u is the stiffness of the bead/actin connection. A similar equation governs movement of the second bead with position $v(t)$. A third equation reflects balance of tension among the compliant bead/actin connections and the surface myosin connection. $[w(t) - v(t)]\gamma_v + [w(t) - u(t)]\gamma_u + Mw(t) = 0$, where γ_v is the stiffness of the bead/actin connection at the end of the actin filament corresponding to $v(t)$ and M is the stiffness of the linkage between the surface and the actin filament, through a single myosin molecule. After using the third equation to eliminate $w(t)$ from the first two, we Fourier transform and solve for $U(f)$ and $V(f)$, each in terms of $F_u(f)$ and $F_v(f)$. These resulting equations are linear with complex, frequency-dependent coefficients. We wish to compute the correlation coefficient between sampled signals $u(n)$ and $v(n)$ reflecting $u(t)$ and $v(t)$ in the time domain. We can compute the Discrete Fourier Transform $U(n/N)$ and $V(n/N)$ by sampling the continuous $U(f)$ and $V(f)$ at fine intervals and extending this by symmetry. Using Parseval's Theorem, we relate the linear correlation coefficient between $u(n)$ and $v(n)$ to the Discrete Fourier Transform

$$r = \Sigma[u(n)\, v(n)]/\sqrt{\Sigma[u^2(n)]\,\Sigma[v^2(n)]} = \Sigma[U(n/N)\, V^*(n/N)]/\sqrt{\Sigma[|U(n/N)|^2]\Sigma[|V(n/N)|^2]}$$

The latter expression can be expanded in terms of $F_u(n/N)$ and $F_v(n/N)$. Because thermal forces acting upon the two beads cannot be correlated, cross-terms like $\Sigma[F_u^*(n/N)\, F_v(n/N)]$ can be dropped. Moreover, because the pattern of heated water molecule collisions with the beads changes faster than all relevant time scales here, $F_u(n/N)$ and $F_v(n/N)$ at every frequency are both equal *on average* to the same constant, and thus they cancel. The resulting expression is a complex sum over digital frequency involving only known parameters, aside from γ_u, γ_v, and M. In the upper graph, we set $M = 0$. The diffusion correlation coefficient now depends on γ_u and γ_v only through a series combination of the two, as expected. The solid line is computed with a solution viscous drag coefficient of $9.42{*}10^{-6}$ g/s. The dotted line is computed with a coefficient twice this value, to account roughly for surface proximity effects on Stoke's Law. As shown, the mapping of stiffness-to-diffusion correlation coefficient does not depend sensitively on the drag coefficient, so surface proximity effects are not significant. The fine, straight lines map the measured diffusion correlation coefficient of 0.45 to a predicted bead-to-bead stiffness of 0.025 pN/nm, which can be compared with the 0.027 pN/nm expected on the basis of position variance measurements. In the lower graph, we use the γ_u and γ_v measured by position variance and allow M to vary between 0 and 1 pN/nm. *Inset* is an expanded area of the marked section on the plot of diffusion correlation coefficient versus M (pN/nm). The fine, straight lines in the *Inset* map the center of the measured diffusion correlation coefficient distribution to 0.65 pN/nm and the extrema of the error range (uncertainty, 0.01; see Fig. 3 legend) to 0.53 and 0.83 pN/nm.

Our values do not agree with the much larger stroke suggested by others in support of loose coupling models (8).

In addition to allowing detection of myosin-binding events, including those not visible in the raw position data, correlated diffusion analysis provides us with a measure of the compliant linkages in the system. One can model the trapped filament as a system of two beads attached to fixed references and to one another by springs (Fig. 1*b*). Over relevant length scales, the bead–filament links appear Hookean, characterized by linear dependence of force on extension, given propagation of triangle waveforms from one bead to the other. Moreover, the Hookean approximation for myosin stiffness is reasonable given the linearity of stress–strain curves measured with single-actin filaments and myosin molecules (11). One can then compute a mapping from spring-element elastic moduli to the expected correlation coefficient between the position of the two beads, allowing one to estimate these moduli from the measured correlation coefficient (Fig. 4). The diffusion correlation coefficients in the absence of bound myosin gave a distribution that peaked at 0.45, indicating a bead-to-bead linkage stiffness of about 0.025 pN/nm. This number is within 10% of the value we compute as a series combination of the two bead-to-surface linkages measured using position variance, further supporting the interpretation that those numbers characterize merely the bead/actin links.

Diffusion correlation coefficients during myosin-binding events show a normal distribution with a mean of 0.05 and uncertainty of 0.01 (increase of χ^2 by 1, method of maximum likelihood). Given stiffness values of both bead/filament links, we can compute a mapping of the stiffness of the surface attachment through myosin to the diffusion correlation coefficient and, thus, estimate this stiffness from the measured correlation. The distribution center indicates that an elastic constraint of 0.65 pN/nm has "broken" the correlation, and the uncertainty maps to a range of 0.53 to 0.83 pN/nm (Fig. 4). These estimates reflect the linkage between the actin filament and the myosin-bound surface, connected through the elasticity of the myosin molecule (16) and its surface attachment. The correlated diffusion technique thus allows us to circumvent the compliant bead/filament linkage, which limits more direct measurements. They are somewhat higher than a previous measurement of rigor head stiffness of 0.58 ± 0.26 pN/nm (11), which was limited by a compliant bead/filament linkage. Unlike this prior measurement, the current one involves a myosin molecule in the midst of an ATPase cycle, bound to actin following its stroke before the binding of ATP. These stiffness measurements allow us to estimate the protein's ability to work against high loads even as we measure the distance moved against low loads by observing bead deflection amplitudes. The probe–filament connections used here are more compliant than the surface linkage of interest, but the correlated diffusion method can be used to detect binding events even when the connections are somewhat stiffer (Fig. 5).

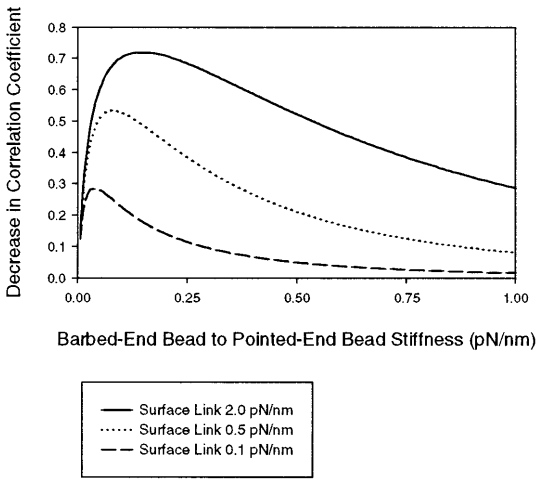

FIG. 5. Loss of correlated diffusion can be applied to detect binding events over a broad range of stiffness values for both the surface-attached protein and the probe–filament connection. Shown here are the computed (as in Fig. 4 legend) drops in the correlation coefficient between thermal diffusion of the two beads when a surface-attached protein binds to the filament. Both traps are assumed to have stiffness of 0.03 pN/nm. The signal is optimized when the probe–filament connections are weaker than the surface linkage, but an observable drop in correlation occurs even when the probe–filament connections are somewhat stronger.

It is intriguing to note that the compliance values measured here predict that the myosin molecule, in its poststroke state under unloaded conditions, will experience significant thermal vibration while still strongly bound to actin, with rms values of 2–3 nm,§ inconsistent with the common notion that the molecule remains tightly clamped after its stroke. It remains possible that myosin supplements the measured 5-nm stroke by rectifying this thermal motion, releasing only when a thermal fluctuation has carried it further in the direction of stroke movement, consistent with A. F. Huxley's original formulation (21). Such extra movement would become visible only just before the myosin molecule detaches, so it would not contribute to the bead deflection data measured here. This is one possible explanation for the fact that the single molecule distance, stiffness, and force measured here and elsewhere (5) predict a myosin thermodynamic efficiency of 3–16%, below the range expected on the basis of whole muscle fiber experiments (22).

The mechanical assay employed here expands the growing range of approaches for examining proteins at the single-molecule level (1–9, 23–26). Our new system allows one to probe the duration and contact stiffness of protein interactions in general, depending only on the ability to link two diffusion probes by an appropriate connecting element. The probe–filament system used here may be generally applied to situations in which a protein of interest either interacts with a filament such as DNA or actin or with a factor that can be engineered in connection with such a filament.

APPENDIX

We observed 387 transient correlation drops, and we sought basically to tabulate events with a flat baseline to either side of a flat plateau in the position data. We constructed six distributions of bead position variance levels, corresponding to regions before, during, and after the diffusion correlation drops on each of the two beads. Each distribution contained a main Gaussian lobe with high-end outliers, and the position variance fluctuates randomly within this range, arguing that the variation in position variance is statistical. The high-end outliers reflected regions of apparent low frequency drift and corresponded to points also outside the main lobe of the correlation coefficient distributions. We truncated the distributions to eliminate these outliers. If an event corresponded to an outlier in any of the six distributions, it was eliminated. Both mean bead deflections remained within 1 nm of their original values as we eliminated events above a threshold variance, with thresholds between 1.5 and 3 standard deviations over the mean variance level. More stringent thresholds begin to infringe on the Gaussian lobe. A threshold of 1.5 standard deviations over the mean eliminated 98 of the original 387 events. Relatively few events exceeded the threshold in any given distribution, although 98 events exceeded it in at least one of the six distributions.

§Computation using equipartition of energy (2).

We gratefully acknowledge K. Eason and B. Simmons for the design of the high-bandwidth I-V conversion circuit used in this experiment. This work was supported by grants from the National Institutes of Health and the Human Frontier Science Program (J.A.S.). A.D.M. is a trainee of the Biophysics Program at Stanford University. J.T.F. was a trainee of the Medical Scientist Training Program at Stanford University School of Medicine.

1. Hinterdorfer, P., Baumgartner, W., Gruber, H. J., Schilcher, K. & Schindler, H. (1996) *Proc. Natl. Acad. Sci. USA* **93,** 3477–3481.
2. Dammer, U., Hegner, M., Anselmetti, D., Wagner, P., Dreier, M., Huber, W. & Guntherodt, H.-J. (1996) *Biophys. J.* **70,** 2437–2441.
3. Svoboda, K., Schmidt, C. F., Schnapp, B. J. & Block, S. M. (1993) *Nature (London)* **365,** 721–727.
4. Finer, J. T., Simmons, R. M. & Spudich, J. A. (1994) *Nature (London)* **368,** 113–119.
5. Molloy, J. E., Burns, J. E., Kendrick-Jones, J., Tregear, R. T. & White, D. C. S. (1995) *Nature (London)* **378,** 209–212.
6. Yin, H., Wang, M. D., Svoboda, K., Landick, R., Block, S. M. & Gelles, J. (1995) *Science* **270,** 1653–1657.
7. Ishijima, A., Harada, Y., Kojima, H., Funatsu, T., Higuchi, H. & Yanagida, T. (1994) *Biochem. Biophys. Res. Commun.* **199,** 1057–1063.
8. Ishijima, A., Kojima, H., Higuchi, H., Harada, Y., Funatsu, T. & Yanagida, T. (1995) *Biophys. J.* **70,** 383–400.
9. Guilford, W. H., Dupuis, D. E., Kennedy, G., Wu, J., Patlak, J. B. & Warshaw, D. M. (1997) *Biophys. J.* **72,** 1006–1021.
10. Kojima, H., Ishijima, A. & Yanagida, T. (1994) *Proc. Natl. Acad. Sci. USA* **91,** 12962–12966.
11. Nishizaka, T., Miyata, H., Yoshikawa, H., Ishiwata, S. & Kinosita, K. (1995) *Nature (London)* **377,** 251–254.
12. Simmons, R. M., Finer, J. T., Chu, S. & Spudich, J. A. (1996) *Biophys. J.* **70,** 1813–1822.
13. White, H. D. & Taylor, E. W. (1976) *Biochemistry* **15,** 5818–5826.
14. Yanagida, T., Arata, T. & Oosawa, F. (1985) *Nature (London)* **316,** 366–369.
15. Ford, L. E., Huxley, A. F. & Simmons, R. M. (1977) *J. Physiol.* **269,** 441–515.
16. Huxley, A. F. & Simmons, R. M. (1971) *Nature (London)* **233,** 533–538.
17. Uyeda, T. Q. P., Kron, S. J. & Spudich, J. A. (1990) *J. Mol. Biol.* **214,** 699–710.
18. Harada, Y. & Yanagida, T. (1988) *Cell Motil. Cytoskeleton* **10,** 71–76.
19. Harada, Y., Sakurada, K., Aoki, T., Thomas, D. D. & Yanagida, T. (1990) *J. Mol. Biol.* **216,** 49–68.
20. Rayment, I., Rypniewski, W. R., Schmidt-Baese, K., Smith, R., Tomchick, D. R., Benning, M. M. & Winkelmann, D. A. (1993) *Science* **261,** 50–58.
21. Huxley, A. F. (1957) *Prog. Biophys. Biophys. Chem.* **7,** 255–318.
22. Woledge, R. C., Curtin, N. A. & Homsher, E. (1985) *Energetic Aspects of Muscle Contraction* (Academic, London).
23. Kuo, S. C. & Sheetz, M. P. (1993) *Science* **260,** 232–234.
24. Howard, J., Hudspeth, A. J. & Vale, R. D. (1989) *Nature (London)* **342,** 154–158.
25. Hunt, S. J., Gittes, G. & Howard, J. (1994) *Biophys. J.* **67,** 766–781.
26. Miyata, H., Hakozaki, H., Yoshikawa, H., Suzuki, N. & Kinosita, K. (1994) *J. Biochem.* **115,** 644–647.